Rock Physics and Depositional Trends*

Marco Perez[1], David Close[1], and Greg Purdue[1]

Search and Discovery Article #41316 (2014)
Posted April 7, 2014

*Adapted from extended abstract prepared in conjunction with presentation at CSPG/CSEG/CWLS GeoConvention 2012, (Vision) Calgary TELUS Convention Centre & ERCB Core Research Centre, Calgary, AB, Canada, 14-18 May 2012, AAPG/CSPG©2014

[1]Apache Canada, Ltd., Calgary, Canada (marco.perez@apachecorp.com)

Abstract

Log based analysis of Lambda-Mu-Rho (LMR) data can predict broad trends in terms of reservoir lithology and hydro-fracture (frack) barrier presence and thickness. Understanding these trends from a rock physics perspective is important as capturing information regarding reservoir properties of interest, such as porosity and Vp:Vs ratio cannot be constrained independently if lithology is unknown. Rock physics has emerged as a tool for geophysicists to characterize reservoir properties as they pertain to seismic elastic parameters. In addition, rock physics models have been presented that relate sedimentology and rock fabric to changes in elastic properties. Through prestack inversion of seismic data, LMR attributes can be used to determine geological trends, elastic parameters of importance as they relate to hydraulic stimulation and reservoir parameters of interest for the purpose of assessing reservoir quality and economic viability.

Introduction

Silt and clay rich lithologies, poor in TOC, are often characterized by distinct sedimentological trends associated with gravity flows and slope failure in many sedimentary basins. Biogenic silica and TOC rich lithologies that often comprise reservoir packages in shale gas plays, in contrast, are characterized by an absence of evidence of large scale transport (although traction flow is likely at the seafloor and observed in core data) and are interpreted to be largely pelagic and show little in terms of grading and/or sedimentary structures.

Rock physics trendlines based on different assumptions about grain sorting and mixing, which can be related to sedimentological trends and ultimately stratigraphy, can be mapped into LMR crossplot space and calibrated to well log data. The influence of mineralogy on data in LMR space is evident; however, beyond this first order mineralogical control on the data are the influences of secondary controls such as rock fabric and fractures. Log data can be used to calibrate rock physics trendlines, but ultimately 3D seismic data, inverted for rock properties, provides the opportunity to map regional geologic trends within a basin and local anomalies at the reservoir scale.

Theory

The conventional seismic interpretation and amplitude versus offset (AVO) inversion workflow provides important information for explorationists. Extending this workflow to quantitatively assess potential rock fabric and grain microstructure provides new opportunities to improve reservoir characterization studies. Rock physics is intrinsically linked to sedimentology through the implicit and explicit assumptions about grain and matrix relationships that are used to describe the material. The conventional applications of such models are primarily related to clastic sequences in which rock fabric and texture relate to grain size and sorting and have compressional and shear velocity expressions. Two different rock physics models will be used to describe rocks:

1. A combination of Hertz-Mindlin contact theory and Hashin-Shtrikman averaging (HMHS), which models quartz–clay mixtures as function of porosity.
2. A bi-modal grain mixture model by Dvorkin and Gutierrez (2002) that models porosity as a function of texture and sorting.

The HMHS formulation is presented by Dvorkin and Nur (1996) and is designed specifically for high-porosity sandstones. For this application, choosing the correct end members is of vital importance as the model is extended to the low porosity end of the trend. The basics of the model consist of defining trend end members (zero porosity and critical porosity) and estimating effective moduli between these end members through the Hashin-Shtrikman bounds. The zero porosity end member is defined by taking a weighted average (Voigt, Reuss, Hill) of the moduli of each mineral component, whereas the critical porosity end member is defined using Hertz-Mindlin contact theory for a random pack of spheres. The expressions for the bulk and shear modulus end members are

$$K_{hm} = \frac{(1-\phi_c)C}{12\pi R} S_N \qquad G_{hm} = \frac{(1-\phi_c)C}{20\pi R}\left(S_N + f\frac{3}{2} S_T \right) \tag{1}$$

where

$$S_N = \frac{4Ga}{1-\nu} \qquad S_T = \frac{8Ga}{2-\nu} \tag{2}$$

and

$$a = R\left[\frac{3\pi(1-\nu)P}{2C(1-\phi_c)G} \right]^{\frac{1}{3}} \tag{3}$$

where *f* is the factor between 0 and 1 relating to the amount of intergranular friction, *C* is the coordination number, *P* is pressure exerted on a grain pack, *v* is Poisson's ratio and *G* is the shear modulus (Duffaut et al., 2010; Bachrach and Avseth, 2008). The end members are then connected by the Hashin-Shtrikman bound which has the form

$$K_{eff} = \left[\frac{\phi/\phi_c}{K_{hm} + 4/3 G_{hm}} + \frac{1-\phi/\phi_c}{K + 4/3 G_{hm}} \right]^{-1} - \frac{4}{3} G_{hm} \quad (4)$$

$$G_{eff} = \left[\frac{\phi/\phi_c}{G_{hm} + Z} + \frac{1-\phi/\phi_c}{G + Z} \right]^{-1} - Z \quad (5)$$

$$Z = \frac{G_{hm}}{6} \frac{9K_{hm} + 8G_{hm}}{K_{hm} + 2G_{hm}} \quad (6)$$

The resulting trends are then mapped into LMR space to be used for interpretation of elastic parameters to infer mineralogy and porosity (Figure 1).

Dvorkin and Gutierrez (2002) introduced a bi-modal grain mixture model, which has two-grain end members, a large grain and a small grain, in which porosity is a function of two distinct conditions:

1. the amount of small grains within the large grain matrix, and
2. the amount of large grains supported within the small grain matrix

This model is extended to low porosity and multi-lithology/multi-mineral cases, suitable for shale gas environments, by creating a number of separate models each accounting for different size and grain composition.

The Dvorkin-Gutierrez (2002) bi-modal model relates the total volume of small grains, when packed together, to the pore space volume of the large grains, when packed together. Figure 2 illustrates the various small and large grain geometries.

The critical porosity geometric configuration is when the pore space of the large grains is equal to the volume of the packed small grains (Figure 2c). When the pore space of the large grains is greater than the volume of the packed small grains, then small grains can reside with the large grain matrix (Figure 2a). This condition can be represented as:

$$\beta \le \phi_{crit} \text{ where } \beta = \frac{r^3 l}{1-\phi_{small}} \Big/ \frac{R^3 L}{1-\phi_{large}} \quad (7)$$

where r is the radius of the small grain, l is the number of small grains in the volume, R is the radius of the large grain and L is the number of large grains in the volume. The total porosity for this geometry is:

$$\phi = \phi_{large} - \beta(1-\phi_{small}) \quad (8)$$

The concentration of small grains, C, in this geometry is β. The alternative scenario occurs when the large grains are suspended in a small grain matrix (Figure 2e), or when $\beta \ge \varphi_{large}$, the concentration of small grains is $C = (1 + (1-\varphi_{large})/\beta)-1$.

To estimate the effective elastic parameters of the large and small grain sequence, the two regimes use different inputs. The Hashin-Shtrikman lower bound is used to estimate elastic properties between the end members and it has the form

$$K_{eff} = \left[\frac{A}{K_A + 4/3\,G_A} + \frac{B}{K_B + 4/3\,G_B}\right]^{-1} - \frac{4}{3}G_C \quad (9)$$

$$G_{eff} = \left[\frac{A}{G_A + Z_A} + \frac{1-B}{G_B + Z_B}\right]^{-1} - Z_C \quad (10)$$

$$Z_s = \frac{G_A}{6}\frac{9K_A + 8G_A}{K_A + 2G_A} \quad (11)$$

The two different regimes are for $\beta \ge \varphi_{crit}$ and $\beta \le \varphi_{crit}$ and inputs to the lower Hashin-Shtrikman bound are shown in Table 1.

Dvorkin and Gutierrez (2002) use the Hertz-Mindlin (Mindlin, 1949) contact theory to estimate the elastic properties of the pure phase. Adjusting for the low porosity of gas shale reservoirs, we propose other methods to estimate the elastic property of the end members. The long wavelength first order scattering method proposed by Kuster and Toksoz (1974), which accounts for distinct pore shapes, is used to estimate the end members, though the Dvorkin et al. (1994) contact cement model can also be used. The Kuster-Toksoz (1974) method was generalized by Berryman (1980) as:

$$\left(K_{KT}^{*}-K_{m}\right)\frac{\left(K_{m}-(4/3)\mu_{m}\right)}{\left(K_{KT}^{*}+(4/3)\mu_{m}\right)}=\sum_{i=1}^{N}x_{i}\left(K_{i}-K_{m}\right)P^{mi} \quad 12)$$

$$\left(\mu_{KT}^{*}-\mu_{m}\right)\frac{\left(\mu_{m}-\zeta_{m}\right)}{\left(\mu_{KT}^{*}+\zeta_{m}\right)}=\sum_{i=1}^{N}x_{i}\left(\mu_{i}-\mu_{m}\right)Q^{mi} \quad 13)$$

where

$$\zeta=\frac{\mu}{6}\frac{\left(9K+8\mu\right)}{\left(K+2\mu\right)}=Z \quad 14)$$

The coefficients P^{mi} and Q^{mi} account for the effects of the different pore shape geometries (Mavko et al., 1994). The results are trends that have distinct shapes in LMR crossplots. Figure 3 shows the Bulk and Shear modulus versus porosity crossplots where the two regimes have distinct trends and how they map out into LMR space. Note that to achieve a bi-modal mixture, the grains need not be large or even of particularly different radii as long as the elastic moduli of the mineral end members are distinct.

The combination of the adapted Dvorkin-Gutierrez model and the HMHS rock physics template helps differentiate between dispersed and laminar type deposition, respectively. Figure 4 shows the two different scenarios that can be modelled in LMR (or any other geophysical) crossplot.

The laminar trend, (modelled by the HMHS rock physics model), shown in the top row of Figure 4, has variable composition from large grain (quartz) to small grain (clay). It would exhibit this trend in LMR space moving from high μρ and low λρ to low μρ and high λρ. In contrast, the dispersive trend would move in LMR space from low λρ and μρ to higher λρ and μρ and then back to lower λρ values. Of importance in the LMR crossplots is not the exact values of λρ and μρ but rather the trends revealed. Panel B in Figure 4 illustrates the point clearly. Both the dispersive and laminar models occupy the same LMR values yet the trends reveal the underlying rock texture and sorting. Using these templates can help interpret prestack inversion for LMR attributes and allow for a more in depth understanding of rock fabric and any associated permeability related to the different depositional mechanisms.

Examples

Consider the following log based plot of the LMR from within the Horn River Basin (Figure 5). Superimposed in color on the crossplots are basic lithology-porosity trendlines derived from the Hertz-Mindlin Hashin-Shtrikman (1963) method outlined by Dvorkin and Nur (1996). Close inspection of the crossplots shows distinct lithological variation. The crossplot shows a large amount of clay influence and has areas of

larger quartz content associated with higher μρ values. In addition, there is clear evidence of limestone influence within the well. Of relevance when interpreting the data is recognizing that points that fall outside the HMHS two mineral model trendlines must have additional mineral inputs to satisfy the measured λρ and μρ values. With seismic data, inverted for LMR parameters (Goodway, 1997), the ability to map out lithological trends is evident.

Using a different trendline focus, Figure 6 shows crossplots from three different wells within the Horn River basin. Attempting to assess the geologic environment or where in the basin these wells are from individually, becomes very difficult if not impossible. However, plotting all wells in the basin by zone, with the depositional trendlines superimposed, reveals a different perspective and foments a geologically plausible interpretation.

The interpretation differences between Zone A and Zone B are as follows:

1) Zone A exhibits a clear carbonate – quartz – clay dispersive trend, which can be seen only when all three wells are plotted together, as well as a component which can be interpreted as laminar deposition
2) Zone B shows more of a carbonate – quartz dispersive trend with a strong limestone component

Note that the data can still be interpreted by the simple, single lithology, rock physics models with equal validity. The dispersive trends, however, provide the possibility to interpret rock fabric and potentially tie into a conceptual or observed geologic framework.

Conclusions

Two rock physics models are used to help interpret log data and can be used to interpret seismic inversions. In LMR crossplot space, two sets of trends are developed and displayed. The first set shows how the first order lithologic effect is represented and the second set shows how depositional trends manifest. These models provide templates for interpreting mineralogical variations as well as provide means to extend geologic models away from well control. It is of great importance that all templates be calibrated against well data and core based analysis.

Acknowledgements

The authors acknowledge the input and suggestions of Howard Pitts.

References Cited

Bachrach, R., and P. Avseth, 2008, Rock physics modeling of unconsolidated sands: Accounting for nonuniform contacts and heterogeneous stress fields in the effective media approximation with applications to hydrocarbon exploration, v. 73/6, p. E197-E209.

Berryman, K.R., 1980, Late Quaternary movement on White Creek Fault, South Island, New Zealand: New Zealand Journal of Geology and Geophysics, v. 23/1, p. 93-101.

Duffaut, K., M. Landro, and R. Sollie, 2010, Using Mindlin theory to model friction-dependent shear modulus in grandular media: Geophysics, v. 75/3, p. E143-E152.

Dvorkin, J., and M.A. Gutierrez, 2002, Grain Sorting, Porosity and Elasticity: Petrophysics, v. 43/3, p. 185-196.

Dvorkin, J., and A. Nur, 1996, Elasticity of high-porosity sandstones: Theory for two North Sea data sets: Geophysics, v. 61/5, p. 1363-1370.

Goodway, B., T. Chen, and J. Downton, 1997, Improved AVO fluid detection and lithology discrimination using Lamé petrophysical parameters; "λρ", "μρ", & "λ/μ fluid stack", from P and S inversions: SEG Expanded Abstracts, v. 16/1, p. 183-186.

Hashin, Z., and S. Shtrikman, 1963, A variational approach to the theory of the elastic behaviour of mulitphase materials: Journal of the Mechanics and Physics of Solids, v. 11/2, p. 127-140.

Kuster, G.T., and N. Toksoz, 1974, Velocity and attenuation of seismic waves in two-phase media: Part I. Theoretical Formulations: Geophysics, v. 39/5, p. 587-606.

Mavko, G., R.C. Nolen-Hoeksema, 1994, Estimating seismic velocities at ultrasonic frequencies in partially saturated rocks: Geophysics, v. 59/2, p. 252-258.

Mindlin, R. D., 1949, Compliance of elastic bodies in contact: Journal of Applied Mechanics: v. 16, p. 259–268.

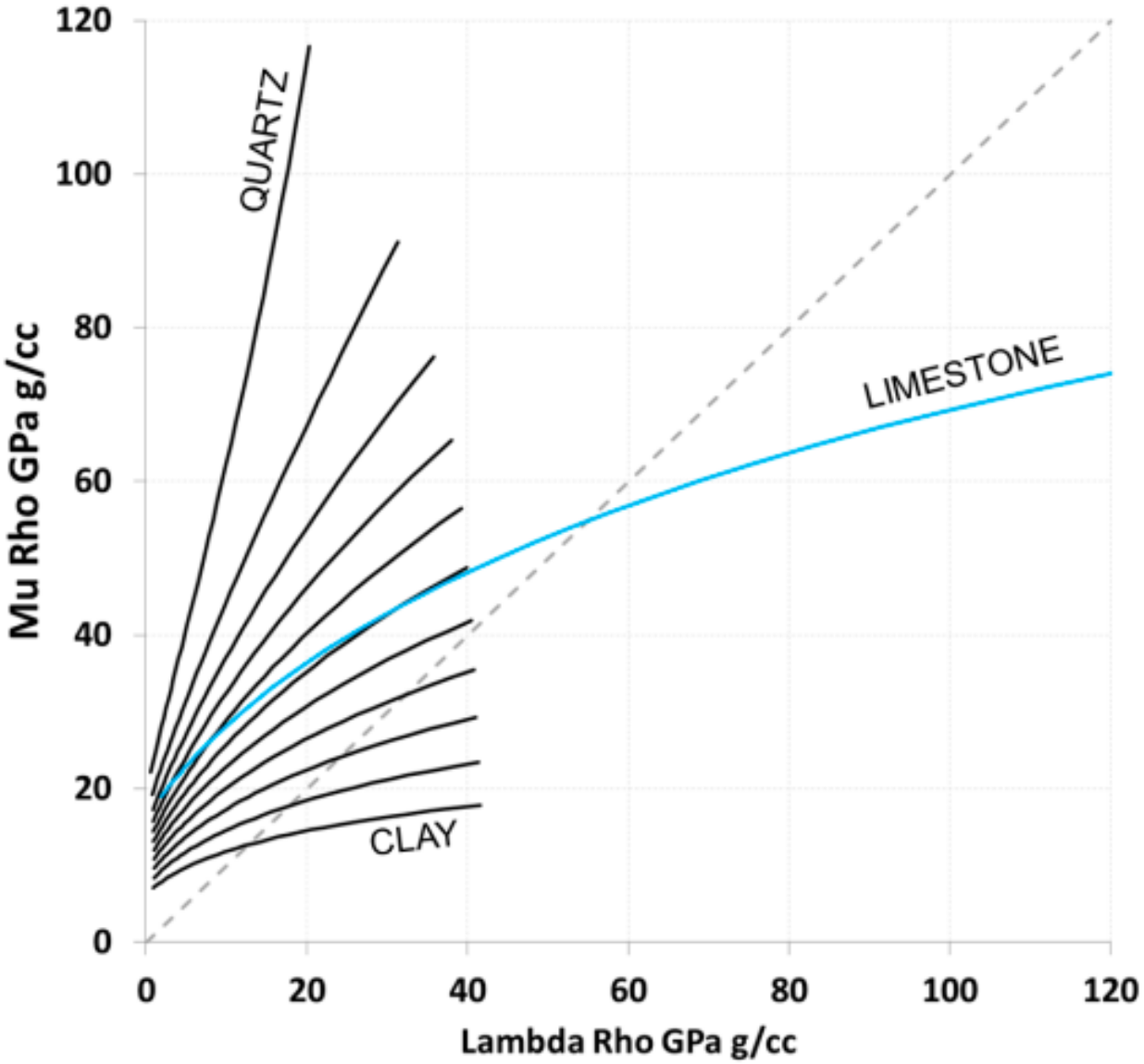

Figure 1. Rock-physics template in LMR for varying quartz-clay mixtures. Each line represents a 10% increase in quartz content from the clay line to the quartz line. A pure limestone trendline is also included (blue line). Note that porosity increases towards the origin.

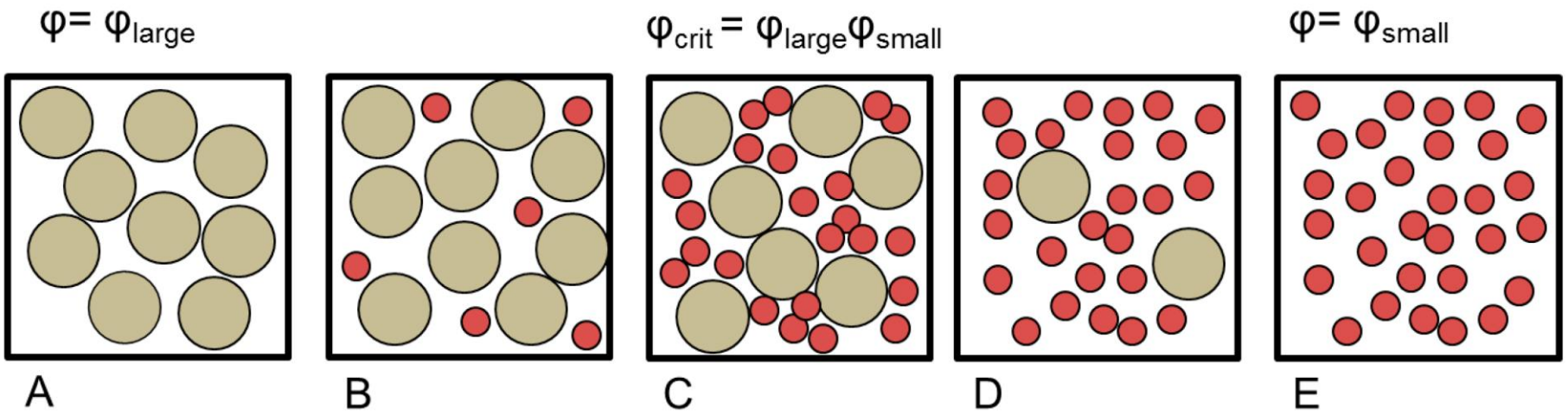

Figure 2. Large and small grain geometries used to model dispersive rock physics model implying rock texture and fabric.

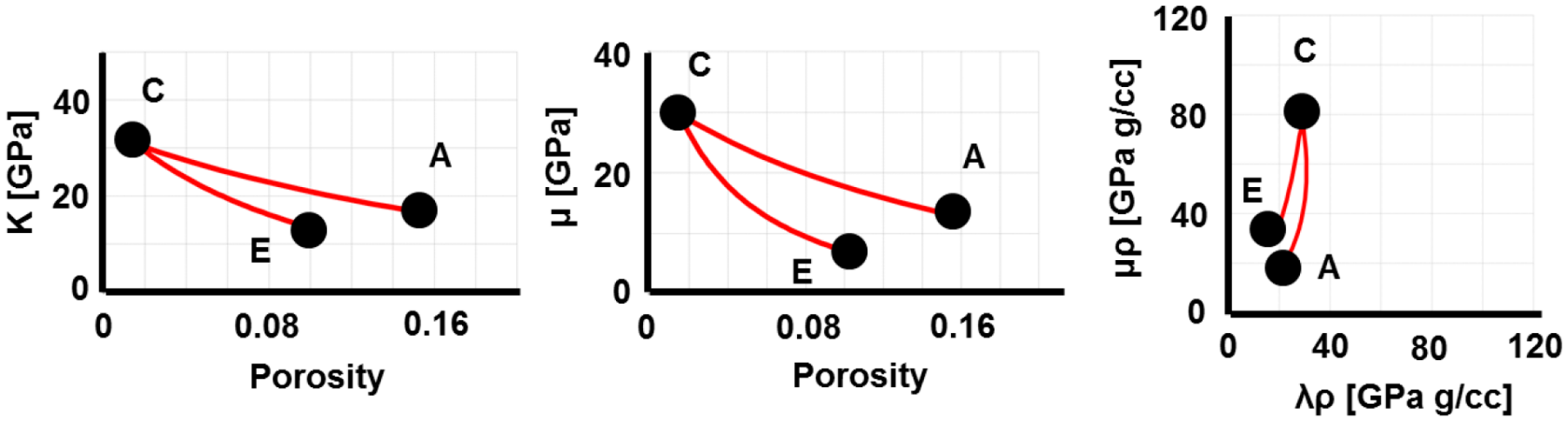

Figure 3. Bulk and shear modulus versus porosity in addition to an LMR crossplot showing bi-modal grain mixture rock physics templates. The points A, C and E refer to the grain geometries in Figure 2.

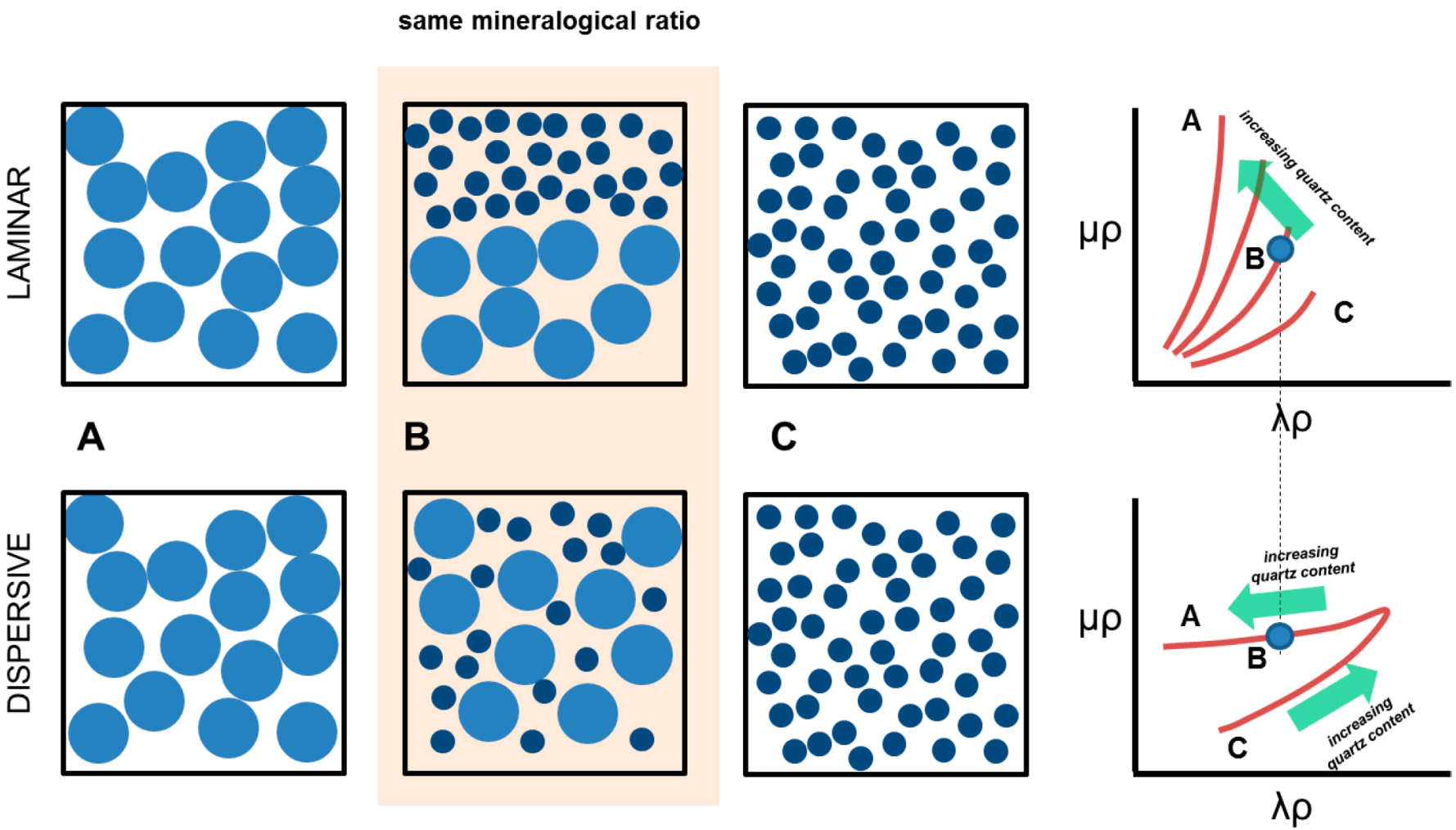

Figure 4. Laminar and dispersive grain geometries and their manifestation in LMR space.

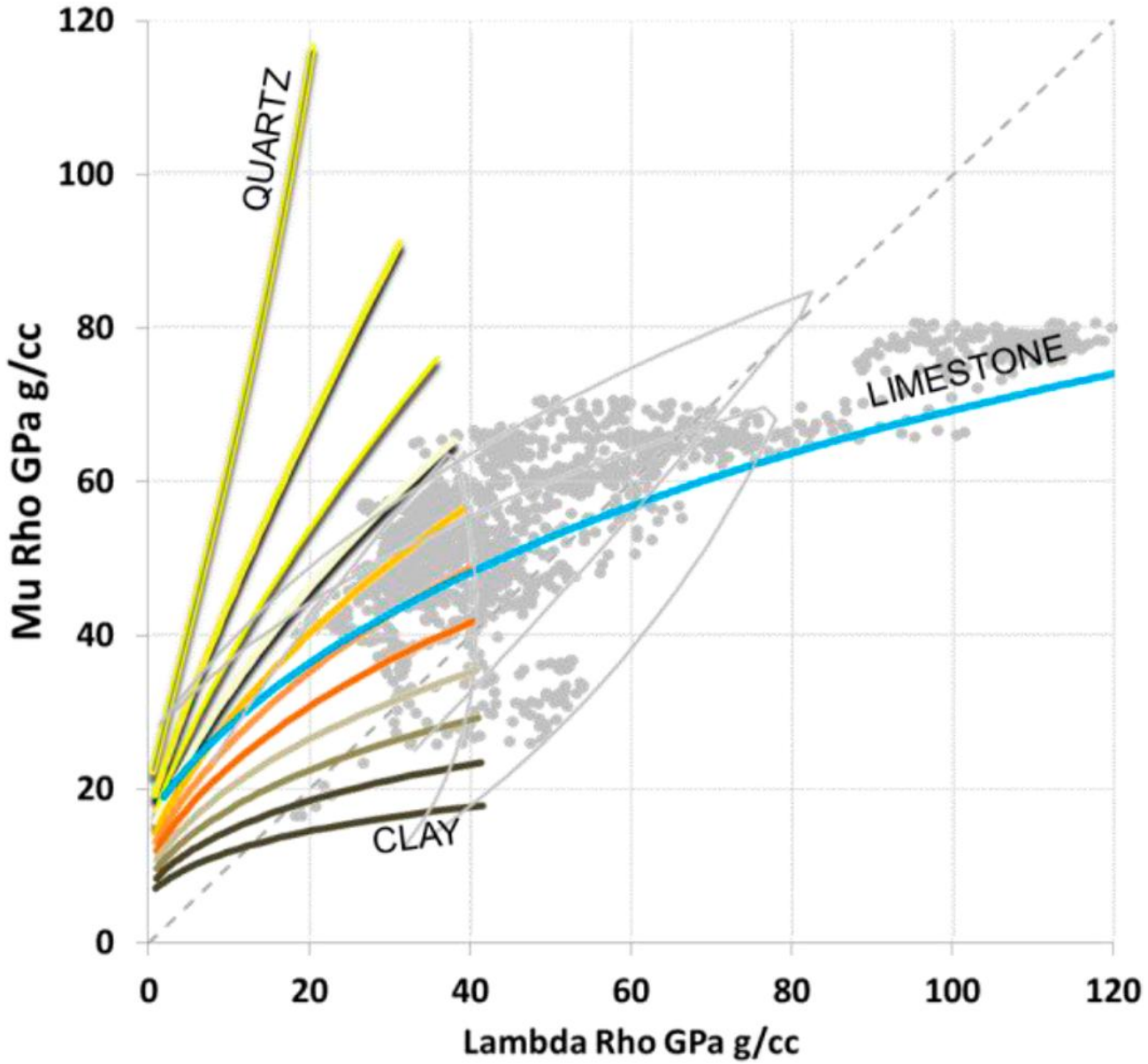

Figure 5. Laminar and dispersive rock physics trends used to help interpret log based seismic attributes of LMR. Laminar trends in color, dispersive trends in grey.

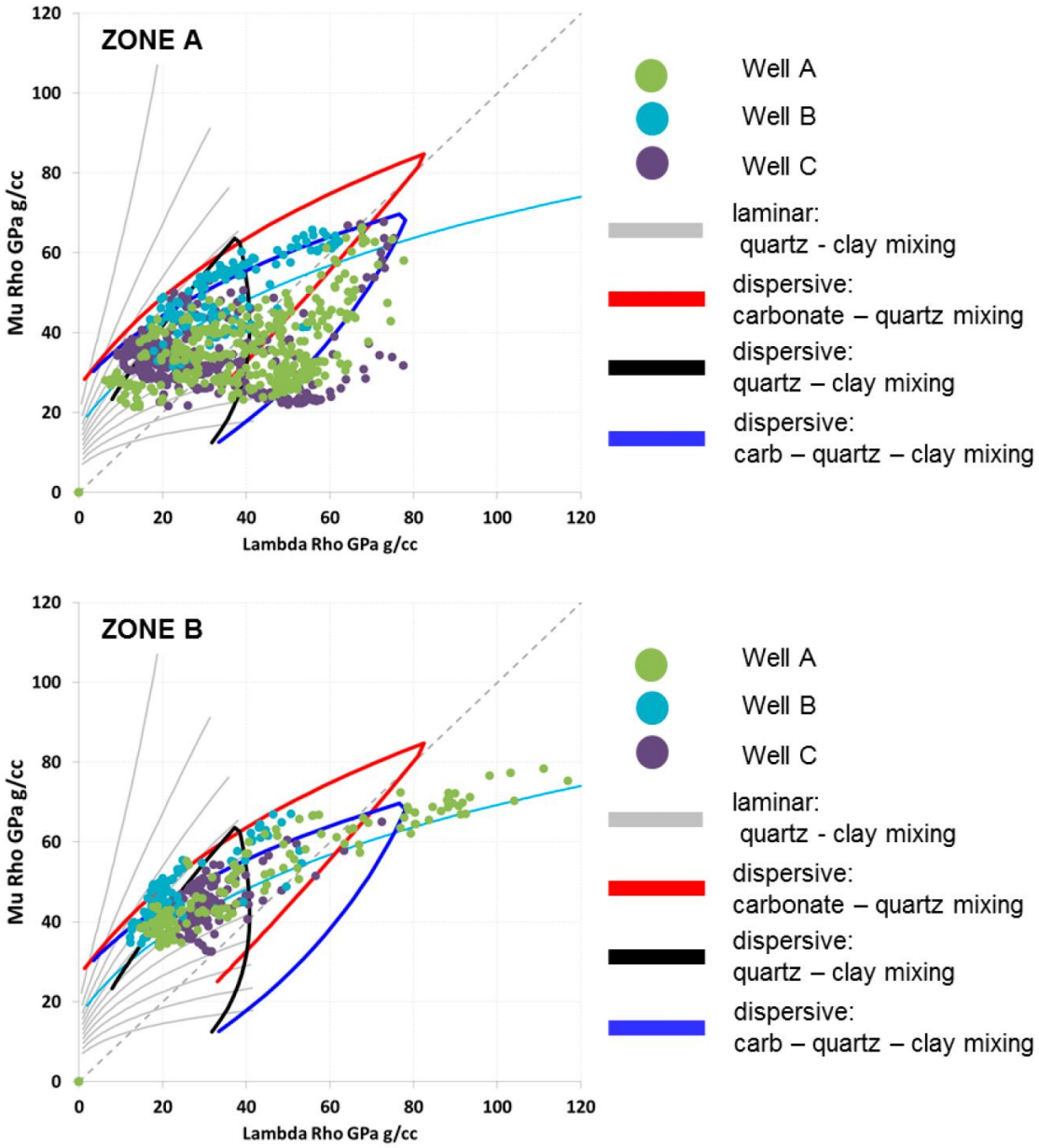

Figure 6. Dispersive and laminar rock physics trends used to help interpret log based seismic attributes of LMR. Laminar trends in grey, dispersive trends in color.

Two regime Bimodal Mixture Inputs				
$\beta \geq \varphi$	$A = C$ $B = 1 - C$	$K_A = K_{small}$ $G_A = G_{small}$	$K_B = K_{large}$ $G_B = G_{small}$	$G_C = G_{small}$
$\beta \leq \varphi$	$A = 1-C/\varphi$ $B = C/\varphi$	$K_A = K_{large}$ $G_A = G_{large}$	$K_B = K_{crit}$ $G_B = G_{large}$	$G_C = G_{large}$

Table 1. Inputs to Hashin-Shtrikman bounds (Equations 9-11) for a bi-modal grain mixture.